

Incorporation of the CORINE land cover dataset into the WRF-NoahMP model

Hajnalka Breuer¹, Ákos János Varga¹, and Zsuzsanna Zempléni¹

¹Eötvös Loránd University

November 23, 2022

Abstract

Land cover information is fundamental in numerical weather prediction and climate modelling because of its impact on the land surface heat, momentum, and moisture fluxes. A new land cover (LC) dataset for the European region is introduced here for the WRF (Weather Research and Forecasting) model coupled with the Noah-MP surface scheme. As part of the Copernicus program the satellite-based Coordination of Information on the Environment (CORINE) LC dataset is available for most of the European continent at high resolution (100 m). This dataset provides a more detailed land cover classification compared to the default WRF LC database over Europe. Its potential applications range from urban numerical studies to regional climate modelling. The CORINE dataset is incorporated into WRF at two different resolutions of 0.00208333° and 0.00416666°. Furthermore, the original 44-category CORINE LC for the WRF model is converted to the USGS LC categories for applications where less detailed but still up-to-date information is desired. It is shown that the application of the CORINE LC dataset not only affects near-surface temperatures (by [?]1 degC on average and [?]3-6 degC over urban areas) but precipitation, snow cover, and wind speed as well.

Incorporation of the CORINE land cover dataset into the WRF-NoahMP model

H. Breuer¹, Á.J. Varga¹, Zs. Zempléni¹

¹Eötvös Loránd University, Pázmány P. s. 1/a, Budapest, Hungary

Key Points:

- Weather Research Forecasting model
- land cover dataset
- Europe

Corresponding author: Hajnalka Breuer, breuer.hajnalka@ttk.elte.hu

Abstract

Land cover information is fundamental in numerical weather prediction and climate modelling because of its impact on the land surface heat, momentum, and moisture fluxes. A new land cover (LC) dataset for the European region is introduced here for the WRF (Weather Research and Forecasting) model coupled with the Noah-MP surface scheme. As part of the Copernicus program the satellite-based Coordination of Information on the Environment (CORINE) LC dataset is available for most of the European continent at high resolution (100 m). This dataset provides a more detailed land cover classification compared to the default WRF LC database over Europe. Its potential applications range from urban numerical studies to regional climate modelling. The CORINE dataset is incorporated into WRF at two different resolutions of 0.00208333° and 0.00416666° . Furthermore, the original 44-category CORINE LC for the WRF model is converted to the USGS LC categories for applications where less detailed but still up-to-date information is desired. It is shown that the application of the CORINE LC dataset not only affects near-surface temperatures (by $\approx 1^\circ\text{C}$ on average and $\approx 3\text{--}6^\circ\text{C}$ over urban areas) but precipitation, snow cover, and wind speed as well.

Plain Language Summary

Weather is generally affected by atmospheric processes; however, it is also impacted by the land surface (e.g., temperatures can differ substantially over dry vs. wet soils or crop fields vs. forests). Such surface information is important to create accurate weather or climate predictions. In this study, we introduce a new, detailed land cover dataset for the European region which could potentially improve numerical simulations of the atmosphere.

1 Introduction

The importance of surface properties in atmospheric modelling is a known conundrum since the '70s. Land-surface features affect the energy budget mainly through the albedo and regulate the energy partitioning between latent and sensible heat flux. The atmospheric effects of different land cover types and subsequent soil moisture availability are widely studied using observations (e.g., Taylor & Lebel, 1998) or numerical modelling (e.g., Avissar & Liu, 1996; Pielke Sr, 2001).

Both numerical weather prediction and climate models utilize land cover information to assign surface properties (e.g., emissivity, stomatal resistance, roughness length) to grid points which are then incorporated into the surface budget calculations (e.g., Niu et al., 2011; Albergel et al., 2012; Masson et al., 2013). A constant improvement of computational resources enables a steady increase in the horizontal resolution of models, which raises the need for a more accurate representation of surface properties. Furthermore, land cover databases require constant updates as urbanization (Liu et al., 2020) and deforestation increases (Ceccherini et al., 2020).

Several studies aim to improve land cover databases regionally (on spatial scales often smaller than a country), which is mostly achieved by a reclassification of the categories to either the original USGS (United States Geological Survey) or to the so-called MODIS (Moderate Resolution Imaging Spectroradiometer) dataset. This relatively simple reclassification nevertheless improves the quality of weather forecasts (De Meij & Vinuesa, 2014; Santos-Alamillos et al., 2015; Unnikrishnan et al., 2016; Sequera et al., 2016; H. Li et al., 2018, 2020) and climate simulations (Gao et al., 2015; Jach et al., 2020). Up-to-date high-resolution land cover datasets are critically important in urban modelling studies (Y. Li et al., 2018; Schicker et al., 2016; Teixeira et al., 2019; Ribeiro et al., 2021) as using proper land cover classes can affect simulated temperatures by more than 4°C .

The WRF model (Skamarock et al., 2019) is an outstandingly convenient tool for land cover research as its source code and static data (geography, land cover, soil texture, albedo, etc.) are freely available and modifiable. The most popular land cover datasets among the WRF community worldwide are the USGS (Loveland et al., 2000) and the IGBP-MODIS (Friedl et al., 2002), generally outdated and lack the necessary spatial heterogeneity outside of the United States. The reclassification of new land cover data (e.g., by the method of Pineda et al. (2004)) to the existing ones does not require source code modification, which makes it a convenient method for updates. As a result of the local/regional updates improvement in 2 m temperature on the order of ± 1 °C and wind on the order of 0.5–1 m/s (e.g., Sequera et al., 2016; López-Espinoza et al., 2020; H. Li et al., 2020) can be achieved, as land cover type affects roughness length and stomatal resistance regardless of the used climatological surface data (e.g., leaf area index, albedo).

The most comprehensive land cover dataset for Europe is the CORINE (Büttner, 2014), which is updated in roughly 3-year intervals. Its native resolution of 100 m enables it to be used for high resolution numerical weather modeling; however, it is only used in models following the reclassification method proposed by Pineda et al. (2004). In this study, the meteorological effects of the application of the CORINE land cover dataset within the WRF model is shown using one-year simulations. In contrast to previous studies (e.g., H. Li et al., 2020), in addition to the reclassified version of the dataset the full CORINE land cover classes are implemented as well. It must be noted, that the implementation is only applicable with the NoahMP (Noah MultiParameterization) surface scheme (Niu et al., 2011) and with the USGS serving as a background land cover dataset.

The study is structured as follows: in Section 2 the applied data is introduced, in Section 3 the methods, the simulation setup, and the implementation of the new classes is described, Section 4 shows the results, and Section 5 concludes the study.

2 Data

2.1 Meteorological data

The WRF simulations cover a 1-year period (2013) in a European domain. Meteorological initial and boundary conditions are provided 6-hourly by the ERA5 (Hersbach et al., 2020) reanalysis dataset. The ERA5 data were downloaded at a horizontal resolution of $0.3^\circ \times 0.3^\circ$, on 37 pressure levels from 1000 hPa to 1 hPa, covering the region 15°N 50°W to 75°N 75°E .

2.2 CORINE land cover

The CORINE project (Büttner, 2014) was initiated in 1985, with the goal to map entire Europe. After the development of a unified methodology including the category system, the scale, and the process of evaluating the recordings, the participating countries work individually to develop the land cover dataset. The database is created at a scale of 1: 100000 (around 100 m) from cartographic databases and satellite imagery. The contribution of the member countries is managed by the European Environment Agency and by 2012 it had been completed in 39 countries for a total of 4 million km^2 . In the CORINE nomenclature (Table S1), there are 44 classes of which 11 refer to artificial, 11 to agricultural, 12 to forest-covered and semi-natural areas. Moreover, there are 5-5 varieties for wetlands and water surfaces. For this study, the 2020 version of the land cover analysis carried out in 2012 is used.

2.3 ESA Land cover

In the CORINE system, the evergreen and deciduous forests are not categorically different, only broad-leaf and coniferous vegetation are distinguished. Nevertheless, to

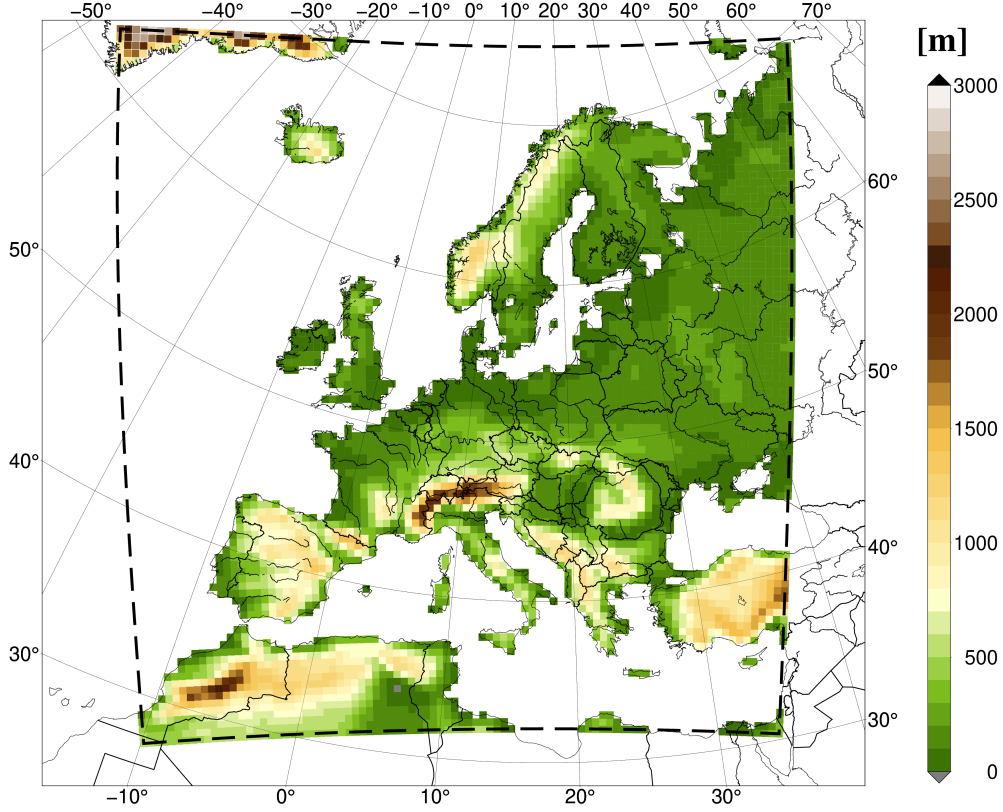


Figure 1. Model domain area and topography at 50 km horizontal resolution

make the distinction, the ESA (European Space Agency) Copernicus Global Land Service global land cover dataset (Buchhorn et al., 2019) was used. Similar to the CORINE dataset, its horizontal resolution is 100 m, but there are only 11 land cover classes. The land cover dataset is available on an annual basis from 2015, from which 2015 was selected as the closest in time to the CORINE land cover dataset.

3 Methods

3.1 WRF Model setup

To test the performance of the new dataset simulations are conducted with the WRF v4.3 (Skamarock et al., 2019) model. The model area encompasses Europe (Fig 1). Despite being available in the CORINE dataset, Eastern Turkey is not covered because of computational and storage limitations. The meteorological simulation take place at a grid with 50 km horizontal resolution. To compare the coverage of the different land cover datasets two higher-resolution (10 km and 2 km) nested domains are utilized, but only used for the presentation of the static data. The number of the domain grid points is 91 x 95, 450 x 475, and 2250 x 2375 for the 50 km, 10 km, and 2 km grid, respectively.

Simulations at 50 km resolution start at 2013-01-01 00 UTC and end at 2013-12-31 00 UTC. Boundary conditions are updated every 6 hours without any reinitialization. Three simulations are introduced in this study, only differing in terms of the land cover dataset used. The reference simulation (REF) employs the Thompson microphysical (Thompson

& Eidhammer, 2014), the RRTMG radiation transfer (Iacono et al., 2008), the Noah-MP surface (Niu et al., 2011), the Bougeault-Lacarrère boundary layer (Bougeault & Lacarrère, 1989), MM5 Monin-Obukhov surface layer (Jiménez et al., 2012), and the Kain-Fritsch cumulus (Kain, 2004) scheme. The simulations run in non-hydrostatic mode, and a time step of 150 s is used for the numerical integration. The COR2USGS simulation refers to the case where the CORINE land cover classes are reclassified into the USGS version using the Pineda et al. (2004) method. The CORINE simulation refers to the case where the complete CORINE classes are used. Leaf area index and albedo values originate from the available climatological monthly fields instead of static table values.

3.2 Incorporation of new land cover data into the WRF model

The CORINE land cover map is first converted with GDAL (GDAL/OGR contributors, 2021) into a compatible netCDF format which includes geographical coordinates. The large file is divided into $2.1^\circ \times 2.1^\circ$ tiles, from which WPS (WRF Preprocessing System) readable 1-bit binary files ($2^\circ \times 2^\circ$ tiles) are created with resolutions of 0.00208333° and 0.00416666° . The ESA Land cover data is similarly divided into $2^\circ \times 2^\circ$ tiles. At grid points where the forest types coincide in the CORINE and ESA sets, the CORINE forests are reclassified from Broad-leaved forest and Coniferous forest to Broad-leaved evergreen forest, Broad-leaved deciduous forest, Coniferous evergreen forest, and Coniferous deciduous forest. As a result, the 44 classes are expanded to 48 classes.

Since the CORINE land cover set does not cover the entire continent, the new classes can only be reasonably incorporated as a secondary land cover layer. When using different layers in land cover data, the type of datasets must be compatible with each other in the preprocessing unit in the WRF model. Because of this, the USGS is chosen as primary and the CORINE as a secondary layer, meaning they can only be used together if the land cover classes are not overlapping. The USGS dataset uses categories from 1 to 33 and from 1 to 41 before and after version 4.3 of WRF, respectively. These include 3 and 11 urban classes, respectively. To leave room for new - e.g., user defined - USGS classes in the future, the new CORINE classes are defined from 51 to 98. This also allows the application for previous model versions; however, slightly different source code modifications are required as there are major changes in the NoahMP parameterization in the latter (4.3) WRF version. There is only one caveat to the CORINE database: the 5 water classes cannot be included. This is because at various locations in the main WRF source code water classes are referred to as one value. The distinction between lakes and other land cover types can nevertheless be made. One unresolved issue with the water class is that in the USGS dataset the Black Sea is categorized as a lake, which is now overwritten with the base water class in the proximity of the seashore. In the CORINE database, valid grid points are only available to a few kilometers into the sea and ocean surfaces creating this slight difference.

Subsequently, the WRF-NoahMP code is modified as there are conditions relating to bare grounds, evergreen-broadleaf vegetation, urban areas, and ice grounds. The conditions now also require 4 additional parameters to be read from the MPTABLE.TBL, referring to the class numbers affected. The MPTABLE (NoahMP model-specific parameters depending on land cover classes) values were left unchanged, but it is possible to change them according to the experience of the user. The modified source codes, parameter tables, and the dataset can be found on Github (<https://github.com/BHajni/WRF-CORINE>) and on Zenodo (10.5281/zenodo.4432128).

The new dataset not only updates the categories but their temporal validity as well. While the USGS dataset refers to the year 1992 and the MODIS to 2001, the CORINE set is valid for 2012.

Figure 2 shows the transition between the USGS and the CORINE datasets based on the dominant classes in every grid point (where CORINE is available) at 50 km and

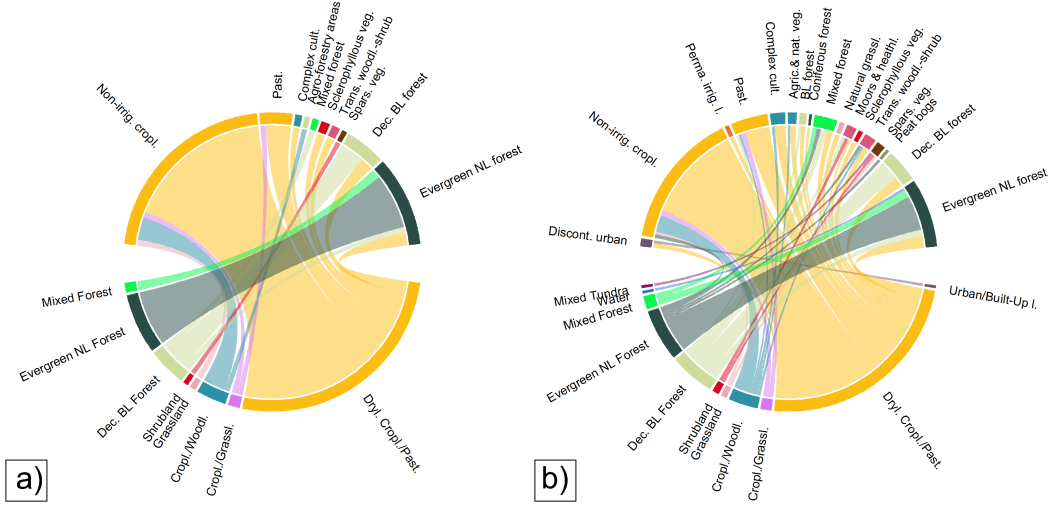


Figure 2. Relationship between the original USGS land cover classes and the CORINE classes, at 50 km (a) and at 2 km (b) resolution. The colors of the nodes correspond to the USGS land cover classes. Only class changes on at least 10, and 6250 grid points are shown, for the 50 km and for the 2 km resolution, respectively. (l. – land, Past. – Pasture, BL – Broad-leaved, NL – Needle-leaved, Dec. – Deciduous, Discont. – Discontinuous, Agric. – Agricultural, veg. – vegetation/vegetated, nat. – natural, irrig. – irrigated, Trans. – Transitional, cult. – cultivation, Spars. – Sparsely)

at 2 km resolution. The resolution unsurprisingly has only a slight effect on the distribution. For example, the agreement between Evergreen needle-leaf forest classes is 86.4% and 68% for 50 km and 2 km resolution, respectively. As can be seen, the most abundant class is the USGS Dryland Cropland/Pasture (Dry-cropland from here) with a relative coverage of 48.6%/42.8%, of which 30.3% (50 km) and 43.1% (2 km) are reassigned depending on the resolution. The reassigned grid points not only end up in related classes such as Pasture but forest areas – both deciduous and evergreen – as well. From all of the USGS Dry-cropland grid points, 8.1%/11% (50 km /2 km) is reclassified to Cropland/Woodland, 8.3%/8% to Deciduous (Dec.) broad-leaf (BL) forest and 5.5%/7.4% to Evergreen needle-leaf (NL) forests. The distribution of class changes depends on land cover types. The spatial differences of dominant categories at 50 km resolution can be seen in Fig S1.

Cropland/Woodland classes are mostly found south of 48.7°N according to the USGS dataset but throughout entire Europe in CORINE, whereas the most changes can be found in the southern European region (Fig 3a). Despite the regional similarity between the USGS and CORINE distribution of Dec. BL forests, most of the new Dec. BL areas can be found south of 55°N. In the case of the Dec. BL forests, the CORINE class comprises 46.2%/43.9% of Dec. BL forests and 40.9%/32% Dry-cropland from the USGS classes. In a similar manner, the CORINE Evergreen NL forest comprises of 58.6%/43.8% Evergreen NL forests, 13.8%/18.3% Cropland/Woodland, 10.9%/10.5% Mixed forests, and 6.3%/10.4% Dec. BL forests. Most of the transitions from Dry-cropland to Evergreen NL can be found in the central European region ($\approx 48^\circ\text{N}/8^\circ\text{E}$ to $55^\circ\text{N}/23^\circ$).

The Cropland/Grassland class (3.5%/4.4% relative coverage in USGS) completely, the Grassland class (2.5%/2.4% relative coverage in USGS) almost completely gets integrated into different CORINE classes. The former is mostly assigned to Dry-cropland

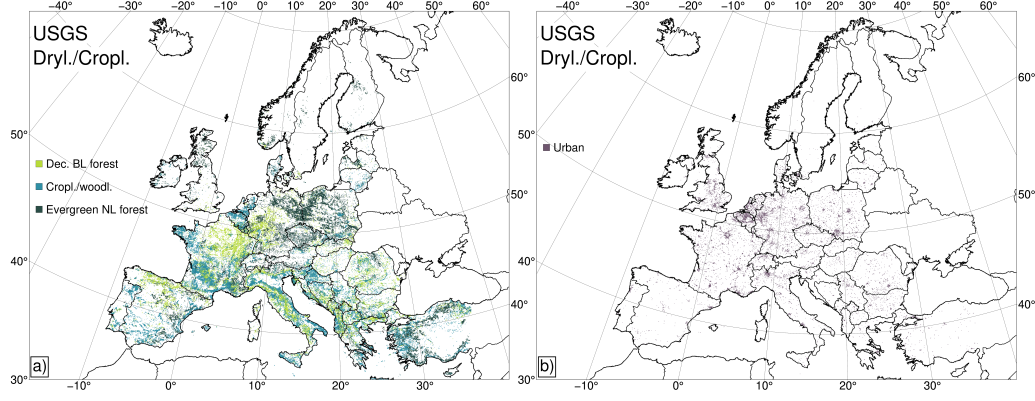


Figure 3. Location of changes from original USGS Dryland/Cropland to the four most frequent other types at 2 km resolution. (l. – land, Dec. – deciduous, BL – broad-leaf, NL – needle-leaf)

and Evergreen NL forests, while the latter to Dry-cropland and Barren/Sparsely vegetated classes.

Although in terms of the relative number of grid points the change from Dry-cropland to urban areas are not significant (0.28%/1.31% of all grid points), the number of urban grid points is multiplied in the CORINE dataset by 9/3.8. An increase in urbanization is most visible (Fig 3b) around the cities of Paris, Milan, Krakow, Katowice, and Warsaw, and also in the regions of Rhineland (Germany) and Brabant (Belgium). Except for the Scandinavian countries (as there are no Dry-cropland classes), there are changes in all CORINE member countries.

The Dec. BL forests cover 9.31%/10.59% of the CORINE region according to the USGS dataset, but only about 48.7%/44.1% of the grid points agree. Of the USGS Dec. BL forest grid points 13.1%/17.1% is assigned to Evergreen NL forests, 8.6%/11% to Mixed forests, and 9%/8.3% to Mixed shrublands. Changes are related to mountain ranges where the Dec. BL forest thrives (> 1500 m above sea level). At 50 km resolution, only areas south to 50°N are affected by the dominant category changes (Fig 4).

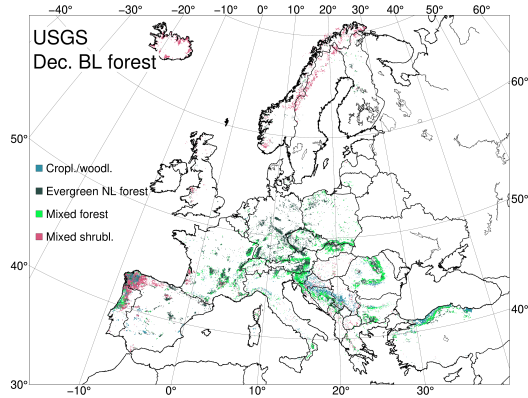


Figure 4. Location of changes from original USGS deciduous (Dec.) broad-leaf (BL) forest to the four most frequent other types at 2 km resolution. (l. – land, NL – needle-leaf)

4 Results

Land cover changes not only impact the magnitude of latent (Fig 5a) and sensible heat fluxes in months with relatively high incoming solar radiation, but also roughness length and thus wind speed throughout the whole year (Fig 5b). Depending on the location and the weather pattern, latent heat changes between the most affected Dry-cropland categories vary with months. According to land cover properties, a conversion from mixed Cropland/Woodland to Dry-cropland should cause a slight increase if the driving meteorological parameters are unchanged as the radiation efficiency driver in the latent heat flux calculations is better for crops. In terms of the conversions from Dry-cropland to woodlands, the largest differences occur when changing to Deciduous BL forests because at the locations of changes the leaf area index (LAI) are the highest (among the changed categories), around $2.8 \text{ m}^2/\text{m}^2$ in summer (Fig S2). The high LAI coupled with the high evapotranspiration efficiencies of crops, enables high latent heat fluxes, creating the largest differences. Similarly, the change to Evergreen NL forests yields the second and to Cropland/Woodland the third largest differences. Throughout the year, the largest differences occur in May-June when the maximum of LAI for the REF Dry-cropland grid points is found.

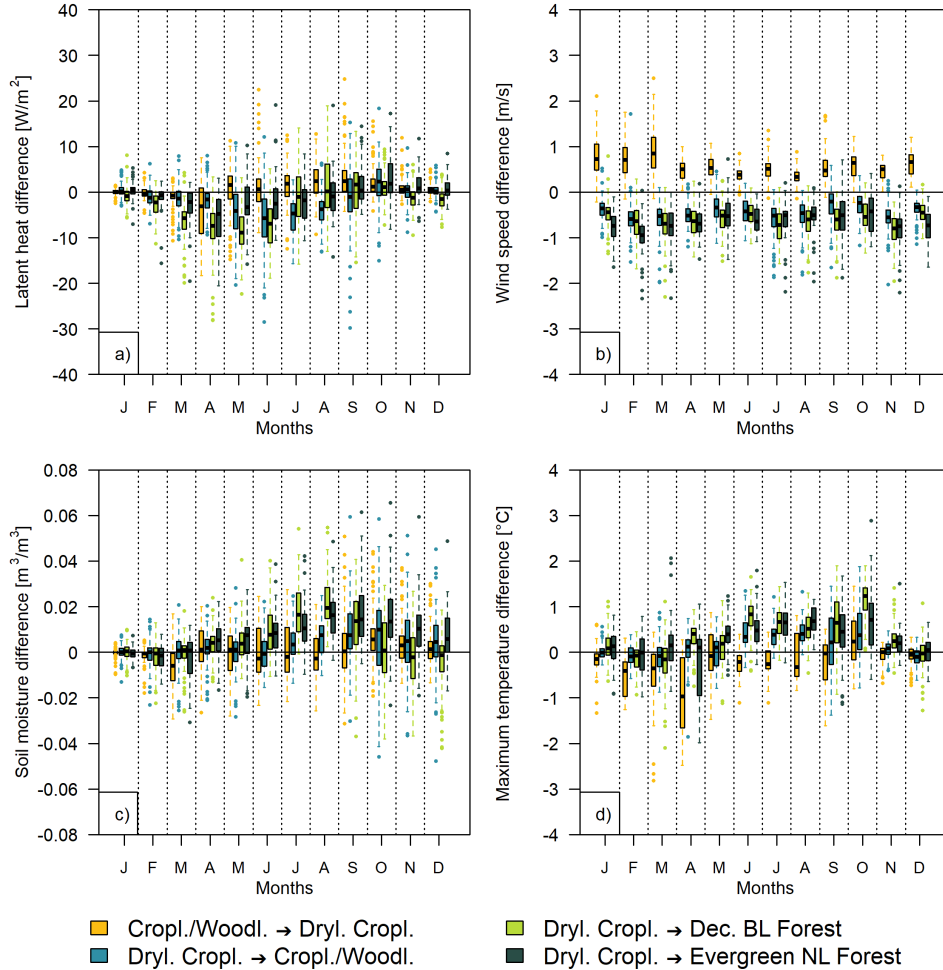


Figure 5. Monthly average differences at grid points of a) latent heat flux, b) wind speed, c) soil moisture, d) maximum temperature between the CORINE reclassified and reference simulations over selected land cover class changes.

Wind speeds differ according to expectations, changing from cropland to woodlands shows a decrease on the order of 0.5 m/s every month. The changing drag and momentum fluxes lead to differing weather patterns even in the first month of the simulation. E.g., a slightly higher (≈ 2 hPa) air pressure is found over Europe (Fig S3).

The lower latent heat flux and the higher interception rate of the forest covers result in higher soil moisture ($\approx 0.02 \text{ m}^3/\text{m}^3$) (Fig 5c). As the year progresses the soil moisture variance increases but it is not the result of diverging precipitation differences (Fig S4a).

Temperature changes are not only determined by the latent heat flux differences but also by the shifting weather patterns. Therefore, the maximum of differences does not coincide with the latent heat releases or differences. Daily average temperatures have their maximal differences in September-October (Fig S4b), just like the daily maximum temperatures (Fig 5d). However, the effect of different latent heat releases is more prominent in the case of daily maximum temperatures. In April the large differences are caused by different predicted snow amounts (≈ 20 cm) and different snow melting rates (≈ 10 – 20 days) (Fig S5,S6). There are only 8 grid points at 50 km resolution where the dominant land cover is changed to urban. At those locations, even without using any urban parameterization, the monthly maximum temperature increases by 2.3°C on average in summer (JJA). However, e.g., in Lisbon (Portugal) the monthly average maximum temperature is 7°C higher in July compared to the REF run (Fig S4c).

Precipitation changes in the whole domain without any specific pattern (Fig 6). The changes in spatial distribution usually show a shift, even when considering the difference between the simulations with the land cover changes (Fig 6a,c). There are some cases when major weather systems change. For example, in September, a Mediterranean cyclone formation is missing in both modified land cover simulations compared to the REF, resulting in significant (over 40 mm difference, about 50% of measured monthly sum) changes in monthly precipitation patterns.

5 Conclusions

A new and updated land cover dataset has been created for the WRF model, applicable specifically for the Noah-MP surface scheme. Aside from the temporal update, the new dataset has more land cover classes which can be important when high-resolution simulations are required. Land cover classes affect the atmospheric processes via roughness length and latent heat flux which can cause changes in large-scale processes when applied over large extents. Temperature differences are around 1°C while changes in monthly precipitation can reach 20–40 mm. It must be noted that the exact differences induced by the new classification depend on the model domain size and configuration, the applied parameterizations, and the dynamical options utilized in model runs.

Acknowledgments

The research leading to this paper was supported by the Hungarian Scientific Research Fund under the grant FK132014. Hajnalka Breuer’s work was additionally financed by the János Bolyai Research Scholarship of the Hungarian Academy of Sciences. Generated using Copernicus Climate Change Service Information [2021]. Neither the European Commission nor ECMWF is responsible for any use that may be made of the Copernicus Information or Data it contains.

The datasets, the modified source codes and tables are free to use and modifiable. The datasets are found at Zenodo: 10.5281/zenodo.4432128, while the model codes are at GitHub: <https://github.com/BHajni/WRF-CORINE>.

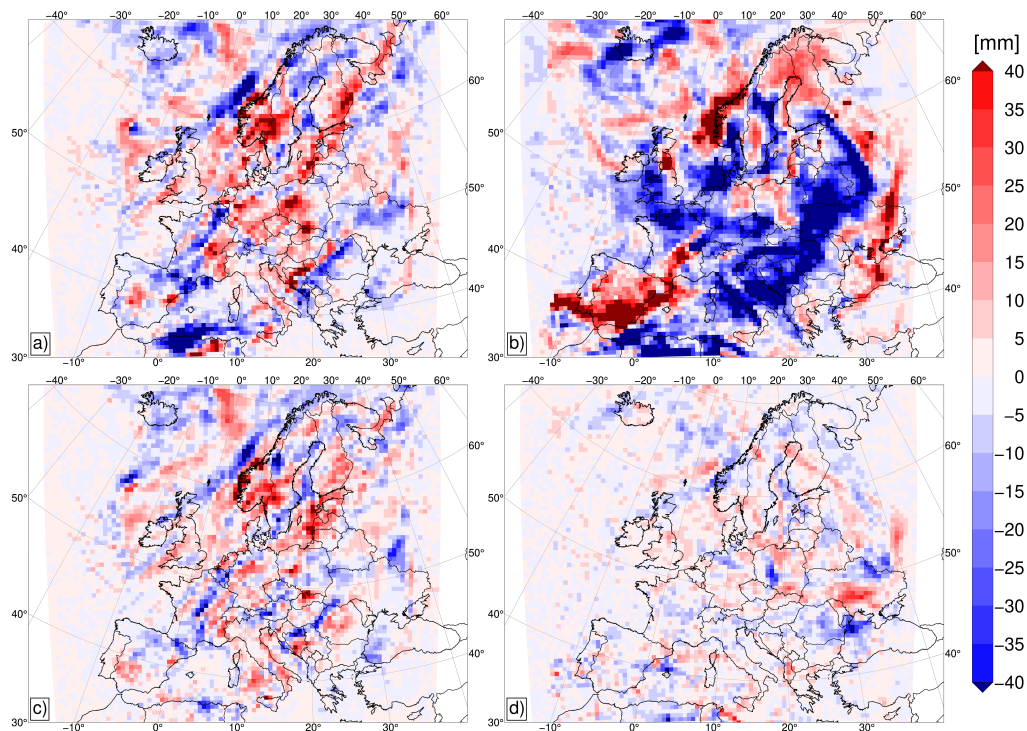


Figure 6. Monthly average precipitation difference between a), b) the full CORINE and reference, c), d) the full and reclassified CORINE land cover simulations, in August and September 2013, respectively

References

- Albergel, C., De Rosnay, P., Balsamo, G., Isaksen, L., & Muñoz-Sabater, J. (2012). Soil moisture analyses at ecmwf: Evaluation using global ground-based in situ observations. *Journal of Hydrometeorology*, 13(5), 1442–1460.
- Avissar, R., & Liu, Y. (1996). Three-dimensional numerical study of shallow convective clouds and precipitation induced by land surface forcing. *Journal of Geophysical Research: Atmospheres*, 101(D3), 7499–7518.
- Bougeault, P., & Lacarrere, P. (1989). Parameterization of orography-induced turbulence in a mesobeta-scale model. *Monthly weather review*, 117(8), 1872–1890.
- Buchhorn, M., Smets, B., Bertels, L., Lesiv, M., Tsendbazar, N.-E., Herold, M., & Fritz, S. (2019, October). *Copernicus Global Land Service: Land Cover 100m: collection 2: epoch 2015: Globe*. Zenodo. Retrieved from <https://doi.org/10.5281/zenodo.3243509> doi: 10.5281/zenodo.3243509
- Büttner, G. (2014). Corine land cover and land cover change products. In *Land use and land cover mapping in europe* (pp. 55–74). Springer.
- Ceccherini, G., Duveiller, G., Grassi, G., Lemoine, G., Avitabile, V., Pilli, R., & Cescatti, A. (2020). Abrupt increase in harvested forest area over europe after 2015. *Nature*, 583(7814), 72–77.
- De Meij, A., & Vinuesa, J. (2014). Impact of srtm and corine land cover data on meteorological parameters using wrf. *Atmospheric Research*, 143, 351–370.
- Friedl, M. A., McIver, D. K., Hodges, J. C., Zhang, X. Y., Muchoney, D., Strahler, A. H., ... others (2002). Global land cover mapping from modis: algorithms and early results. *Remote sensing of Environment*, 83(1-2), 287–302.
- Gao, Y., Weiher, S., Markkanen, T., Pietikäinen, J.-P., Gregow, H., Henttonen,

- H. M., ... Laaksonen, A. (2015). Implementation of the corine land use classification in the regional climate model remo. *Boreal environment research*, 20, 261–282.
- GDAL/OGR contributors. (2021). GDAL/OGR geospatial data abstraction software library [Computer software manual]. Retrieved from <https://gdal.org>
- Hersbach, H., Bell, B., Berrisford, P., Hirahara, S., Horányi, A., Muñoz-Sabater, J., ... others (2020). The era5 global reanalysis. *Quarterly Journal of the Royal Meteorological Society*, 146(730), 1999–2049.
- Iacono, M. J., Delamere, J. S., Mlawer, E. J., Shephard, M. W., Clough, S. A., & Collins, W. D. (2008). Radiative forcing by long-lived greenhouse gases: Calculations with the aer radiative transfer models. *Journal of Geophysical Research: Atmospheres*, 113(D13).
- Jach, L., Warrach-Sagi, K., Ingwersen, J., Kaas, E., & Wulfmeyer, V. (2020). Land cover impacts on land-atmosphere coupling strength in climate simulations with wrf over europe. *Journal of Geophysical Research: Atmospheres*, 125(18), e2019JD031989.
- Jiménez, P. A., Dudhia, J., González-Rouco, J. F., Navarro, J., Montávez, J. P., & García-Bustamante, E. (2012). A revised scheme for the wrf surface layer formulation. *Monthly Weather Review*, 140(3), 898–918.
- Kain, J. S. (2004). The kain–fritsch convective parameterization: an update. *Journal of applied meteorology*, 43(1), 170–181.
- Li, H., Wolter, M., Wang, X., & Sodoudi, S. (2018). Impact of land cover data on the simulation of urban heat island for berlin using wrf coupled with bulk approach of noah-lsm. *Theoretical and applied climatology*, 134(1), 67–81.
- Li, H., Zhang, H., Mamtimin, A., Fan, S., & Ju, C. (2020). A new land-use dataset for the weather research and forecasting (wrf) model. *Atmosphere*, 11(4), 350.
- Li, Y., Zhao, C., Zhang, T., Wang, W., Duan, H., Liu, Y., ... Pu, Z. (2018). Impacts of land-use data on the simulation of surface air temperature in north-west china. *Journal of Meteorological Research*, 32(6), 896–908.
- Liu, X., Huang, Y., Xu, X., Li, X., Li, X., Ciais, P., ... others (2020). High-spatiotemporal-resolution mapping of global urban change from 1985 to 2015. *Nature Sustainability*, 3(7), 564–570.
- López-Espinoza, E. D., Zavala-Hidalgo, J., Mahmood, R., & Gómez-Ramos, O. (2020). Assessing the impact of land use and land cover data representation on weather forecast quality: A case study in central mexico. *Atmosphere*, 11(11), 1242.
- Loveland, T. R., Reed, B. C., Brown, J. F., Ohlen, D. O., Zhu, Z., Yang, L., & Merchant, J. W. (2000). Development of a global land cover characteristics database and igbp discover from 1 km avhrr data. *International Journal of Remote Sensing*, 21(6-7), 1303–1330.
- Masson, V., Le Moigne, P., Martin, E., Faroux, S., Alias, A., Alkama, R., ... others (2013). The surfexv7. 2 land and ocean surface platform for coupled or offline simulation of earth surface variables and fluxes. *Geoscientific Model Development*, 6(4), 929–960.
- Niu, G.-Y., Yang, Z.-L., Mitchell, K. E., Chen, F., Ek, M. B., Barlage, M., ... others (2011). The community noah land surface model with multiparameterization options (noah-mp): 1. model description and evaluation with local-scale measurements. *Journal of Geophysical Research: Atmospheres*, 116(D12).
- Pielke Sr, R. A. (2001). Influence of the spatial distribution of vegetation and soils on the prediction of cumulus convective rainfall. *Reviews of Geophysics*, 39(2), 151–177.
- Pineda, N., Jorba, O., Jorge, J., & Baldasano, J. (2004). Using noaa avhrr and spot vgt data to estimate surface parameters: application to a mesoscale meteorological model. *International journal of remote sensing*, 25(1), 129–143.
- Ribeiro, I., Martilli, A., Falls, M., Zonato, A., & Villalba, G. (2021). Highly resolved

- 357 wrf-bep/bem simulations over barcelona urban area with lcz. *Atmospheric Re-*
 358 *search*, 248, 105220.
- 359 Santos-Alamillos, F., Pozo-Vázquez, D., Ruiz-Arias, J., & Tovar-Pescador, J. (2015).
 360 Influence of land-use misrepresentation on the accuracy of wrf wind estimates:
 361 Evaluation of glcc and corine land-use maps in southern spain. *Atmospheric*
 362 *Research*, 157, 17–28.
- 363 Schicker, I., Arias, D. A., & Seibert, P. (2016). Influences of updated land-use
 364 datasets on wrf simulations for two austrian regions. *Meteorology and Atmo-*
 365 *spheric Physics*, 128(3), 279–301.
- 366 Sequera, P., González, J. E., McDonald, K., LaDochy, S., & Comarazamy, D. (2016).
 367 Improvements in land-use classification for estimating daytime surface temper-
 368 atures and sea-breeze flows in southern california. *Earth Interactions*, 20(16),
 369 1–32.
- 370 Skamarock, W. C., Klemp, J. B., Dudhia, J., Gill, D. O., Liu, Z., Berner, J., . . .
 371 others (2019). A description of the advanced research wrf model version 4.
 372 *National Center for Atmospheric Research: Boulder, CO, USA*, 145.
- 373 Taylor, C. M., & Lebel, T. (1998). Observational evidence of persistent convective-
 374 scale rainfall patterns. *Monthly Weather Review*, 126(6), 1597–1607.
- 375 Teixeira, J., Fallmann, J., Carvalho, A., & Rocha, A. (2019). Surface to boundary
 376 layer coupling in the urban area of lisbon comparing different urban canopy
 377 models in wrf. *Urban Climate*, 28, 100454.
- 378 Thompson, G., & Eidhammer, T. (2014). A study of aerosol impacts on clouds and
 379 precipitation development in a large winter cyclone. *Journal of the atmospheric*
 380 *sciences*, 71(10), 3636–3658.
- 381 Unnikrishnan, C., Gharai, B., Mohandas, S., Mamgain, A., Rajagopal, E., Iyen-
 382 gar, G. R., & Rao, P. (2016). Recent changes on land use/land cover over
 383 indian region and its impact on the weather prediction using unified model.
 384 *Atmospheric Science Letters*, 17(4), 294–300.

Supporting Information for "Incorporation of the CORINE land cover dataset into the WRF-NoahMP model"

H. Breuer¹, Á.J. Varga¹, Zs. Zempléni¹

¹Eötvös Loránd University, Pázmány P. s. 1/a, Budapest, Hungary

Contents of this file

1. Table S1
2. Figures S1 to S6
3. Text S1

Introduction

This supporting information file mostly include figures for a more detailed analysis of the results. The supplemental table includes the list of land cover class names.

Text S1. Snow depth data refers to the Copernicus Global Land Service's (CGLS) snow water equivalent product at 0.05° resolution. The dataset is created by using satellite and station snow depth measurements (Takala et al., 2011; Pulliainen, 2006). From the snow water equivalent, snow depth is can be calculated using a constant 240 kg m^{-3} snow density.

References

- Pulliainen, J. (2006). Mapping of snow water equivalent and snow depth in boreal and sub-arctic zones by assimilating space-borne microwave radiometer data and ground-based observations. *Remote sensing of Environment*, 101(2), 257–269.
- Takala, M., Luojus, K., Pulliainen, J., Derksen, C., Lemmetyinen, J., Kärnä, J.-P., ... Bojkov, B. (2011). Estimating northern hemisphere snow water equivalent for climate research through assimilation of space-borne radiometer data and ground-based measurements. *Remote Sensing of Environment*, 115(12), 3517–3529.

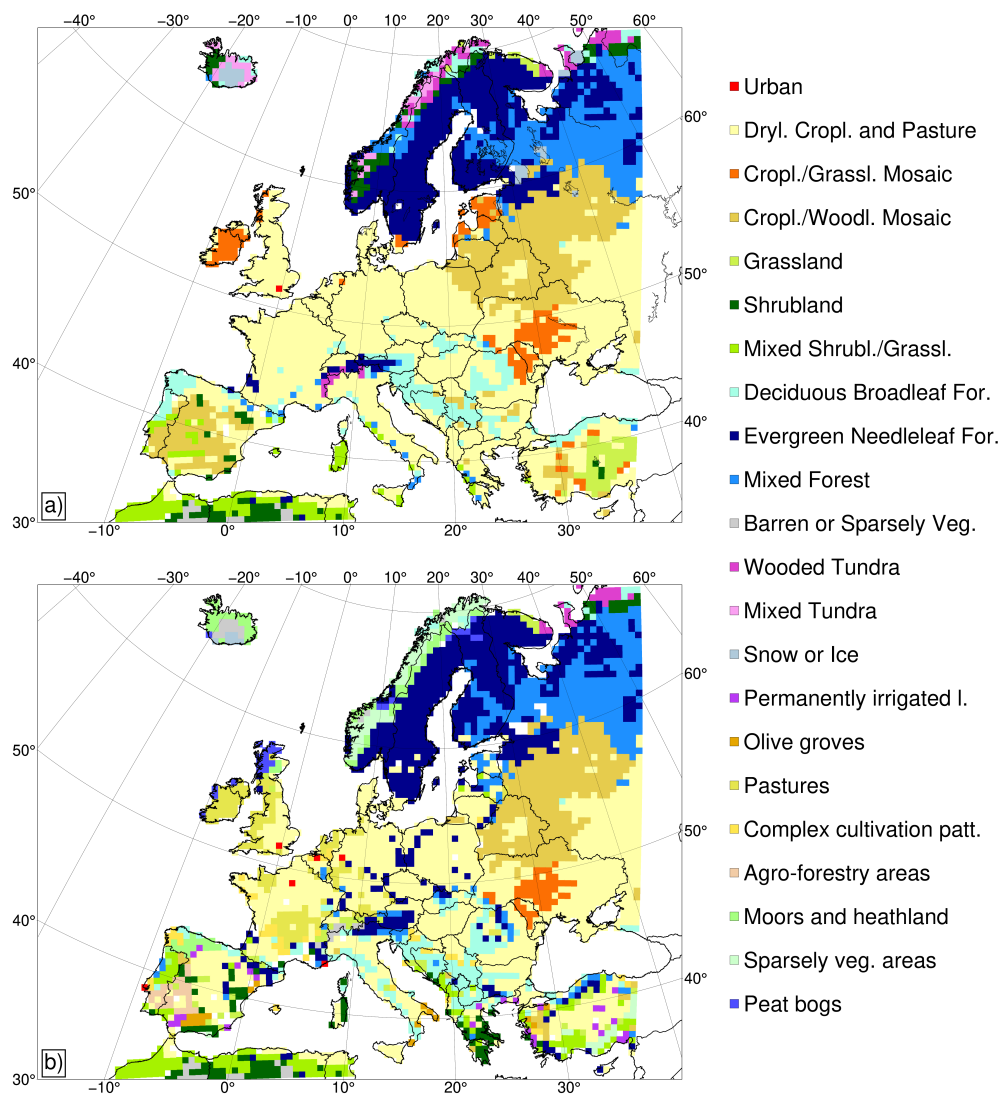


Figure S1. Dominant land cover categories at 50 km resolution over landmass based on a) USGS, b) CORINE database. With the exception of urban category, only categories with at least 5 grid point coverage are colored.

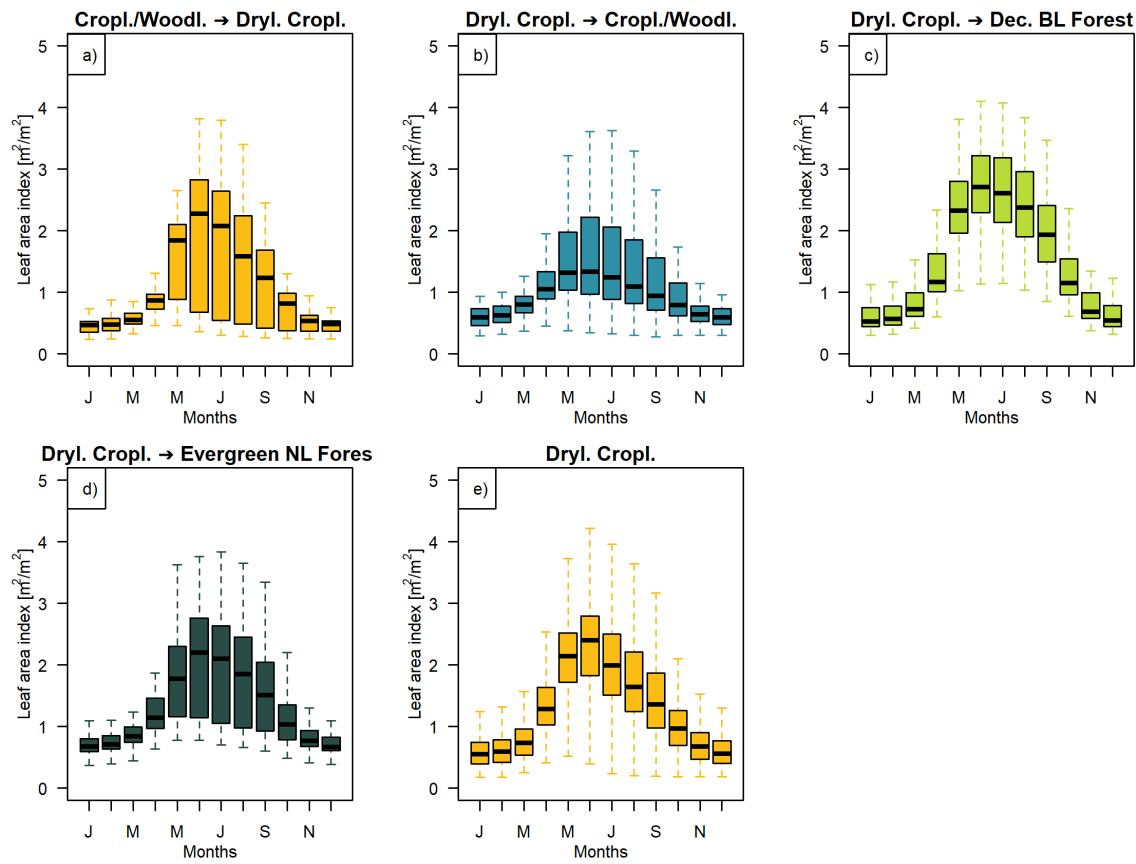


Figure S2. Monthly leaf area index at grid points with the indicated land cover change between the reclassified CORINE and the reference simulation.

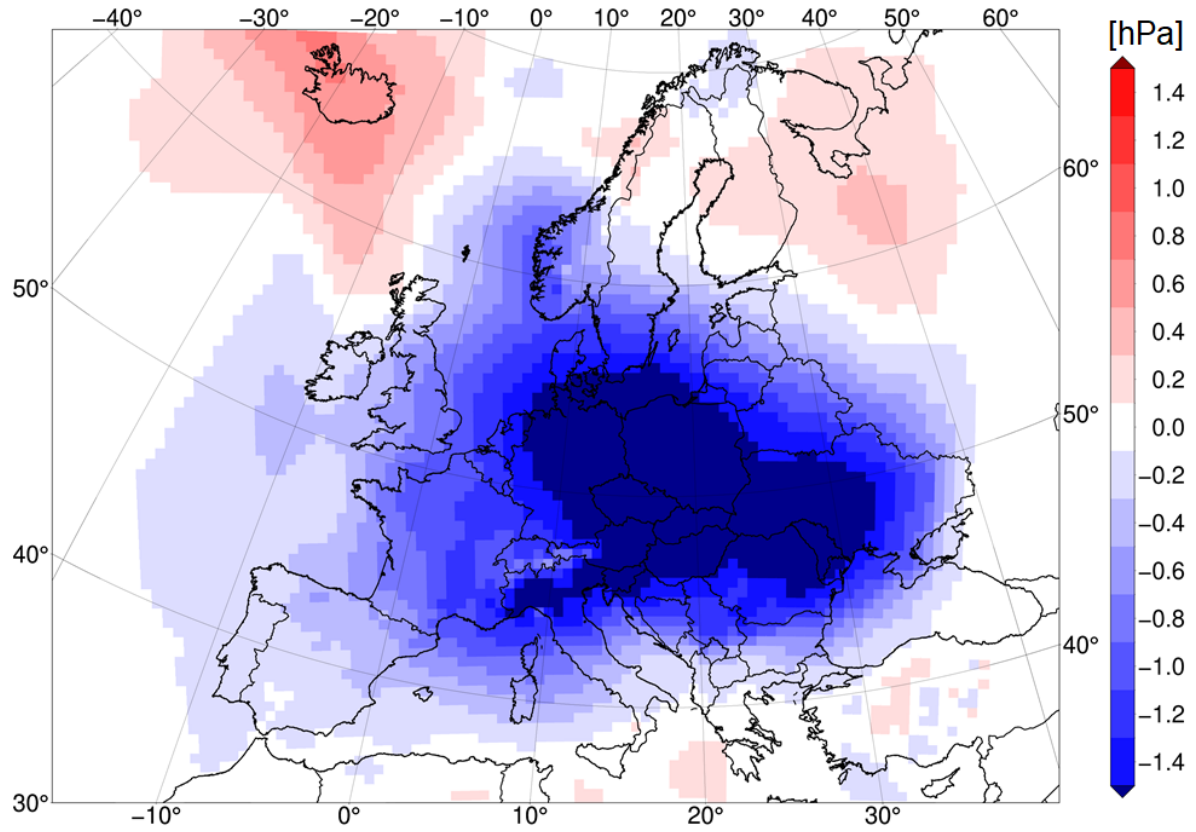


Figure S3. January average mean sea level pressure difference [hPa] between reclassified CORINE and reference simulation

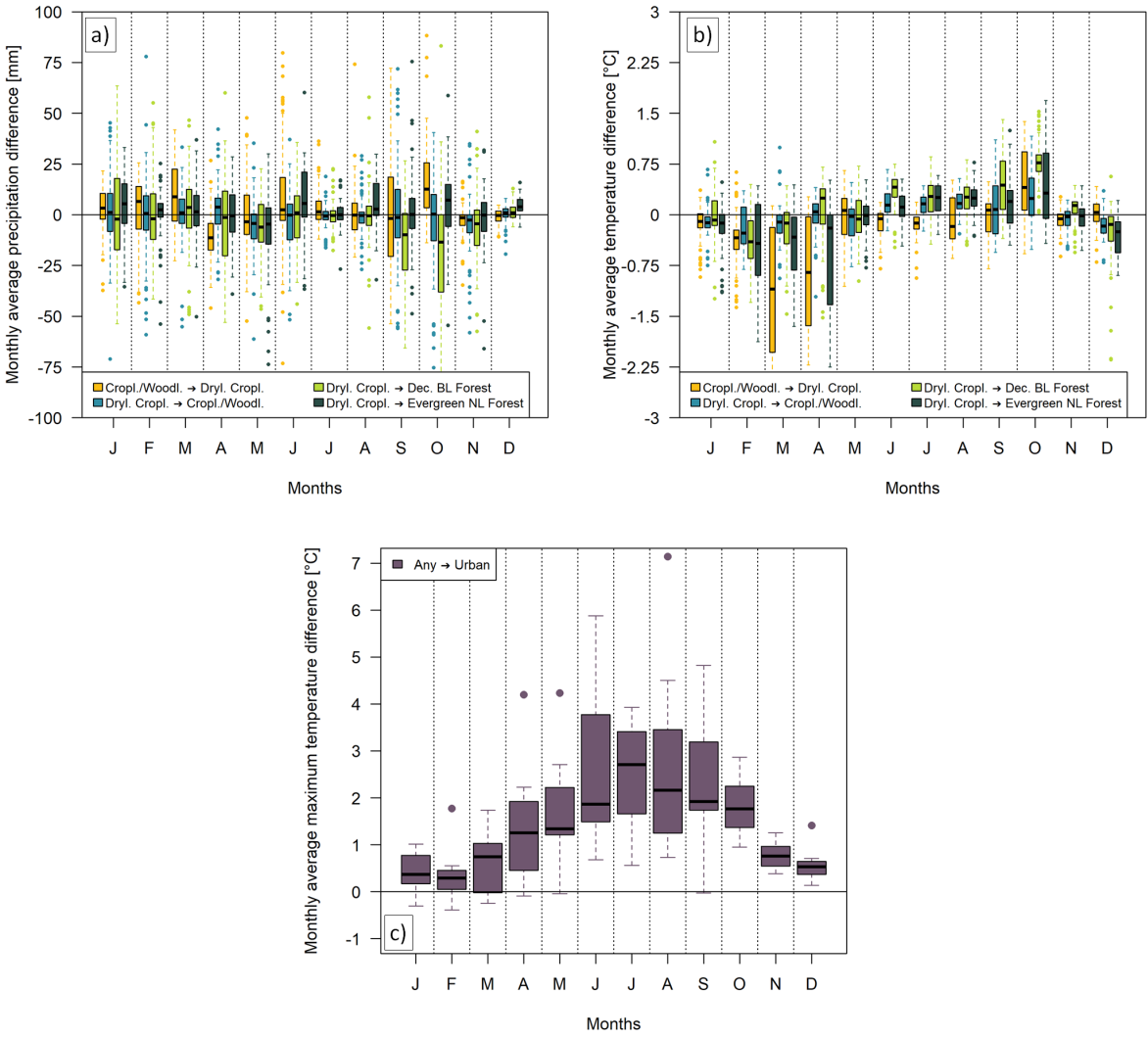


Figure S4. Monthly differences at grid points of a) precipitation [mm], b) temperature at 2 m [°C], c) maximum temperature at 2 m [°C] between the CORINE reclassified and reference simulations over selected land cover class changes.

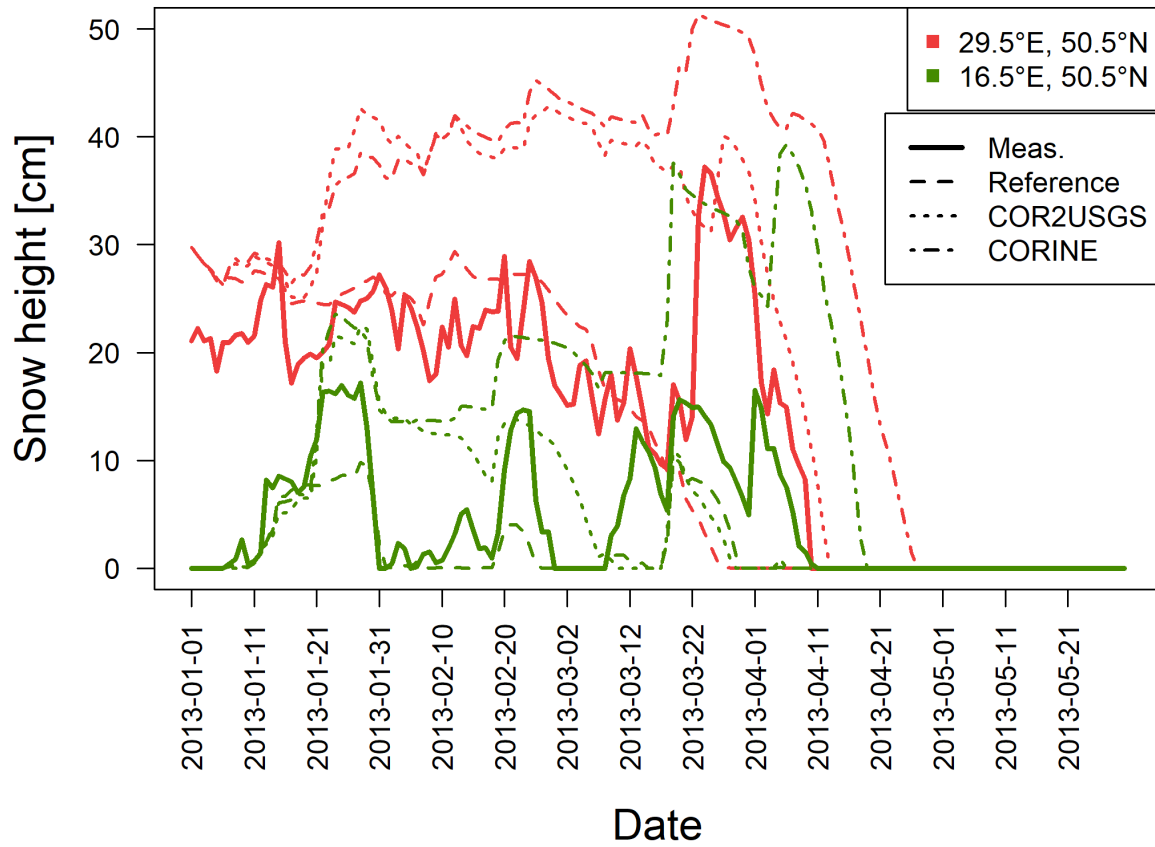


Figure S5. Snow height at two locations based on satellite measurements and on the three simulations. (29.5°E, 50.5°N: Central Dnieper Upland, Ukraine; 16.5°E, 50.5°N: Central Sudetes, Poland).

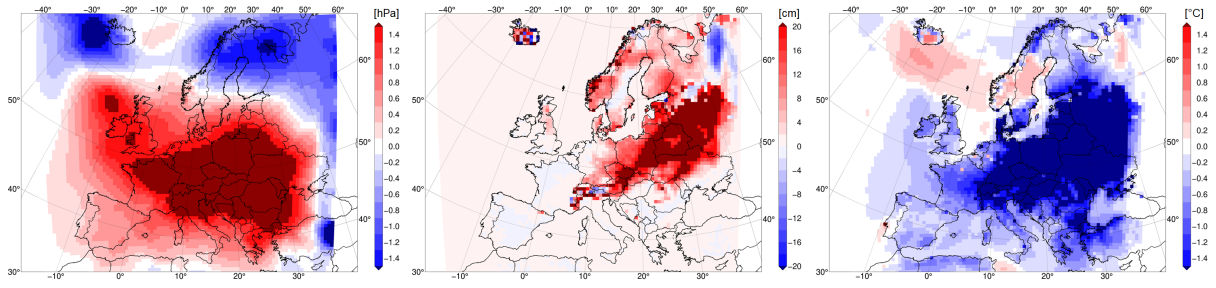


Figure S6. Monthly average difference between the full CORINE and reference simulation in April 2013 for a) sea level pressure [hPa], b) snow height [cm], c) temperature [°C].